

1 Article

2 

# Single-Electron Redox Chemistry on the $[\text{Cp}^*\text{Rh}]$ 3 Platform Enabled by a Nitrated Bipyridyl Ligand

4 **William N. G. Moore,<sup>1</sup> Wade C. Henke,<sup>1</sup> Davide Lionetti,<sup>1</sup> Victor W. Day,<sup>1</sup> and James D.  
5 Blakemore<sup>1,\*</sup>**6 <sup>1</sup> Department of Chemistry, University of Kansas, 1251 Wescoe Hall Drive, Lawrence, Kansas 66045, United  
7 States

8 \* Correspondence: blakemore@ku.edu

9 Received: date; Accepted: date; Published: date

10 **Abstract:**  $[\text{Cp}^*\text{Rh}]$  complexes ( $\text{Cp}^*$  = pentamethylcyclopentadienyl) are attracting renewed interest  
11 in coordination chemistry and catalysis, but these useful compounds often undergo net  
12 two-electron redox cycling that precludes observation of individual one-electron reduction events.  
13 Here, we show that a  $[\text{Cp}^*\text{Rh}]$  complex bearing the 4,4'-dinitro-2,2'-bipyridyl ligand (dnbpy) (3)  
14 can access a distinctive manifold of five oxidation states in organic electrolytes, contrasting with  
15 prior work that found no accessible reductions in aqueous electrolyte. These states are readily  
16 generated from a newly isolated and fully characterized rhodium(III) precursor complex 3,  
17 formulated as  $[\text{Cp}^*\text{Rh}(\text{dnbpy})\text{Cl}]\text{PF}_6$ . Single-crystal X-ray diffraction data, previously unavailable  
18 for the dnbpy ligand bound to the  $[\text{Cp}^*\text{Rh}]$  platform, confirm the presence of both  $[\eta^5\text{-Cp}^*]$  and  
19  $[\kappa^2\text{-dnbpy}]$ . Four individual one-electron reductions of 3 are observed, contrasting sharply with  
20 the single two-electron reductions of other  $[\text{Cp}^*\text{Rh}]$  complexes. Chemical preparation and study of  
21 the singly reduced species with electronic absorption and electron paramagnetic resonance  
22 spectroscopies indicate that the first reduction is predominantly centered on the dnbpy ligand.  
23 Comparative cyclic voltammetry studies with  $[\text{NBu}_4]\text{[PF}_6]$  and  $[\text{NBu}_4]\text{[Cl]}$  as supporting  
24 electrolytes indicate that the chloride ligand can be lost from 3 by ligand exchange upon reduction.  
25 Spectroelectrochemical studies with UV-visible detection reveal isosbestic behavior, confirming  
26 the clean interconversion of the reduced forms of 3 inferred from the voltammetry with  
27  $[\text{NBu}_4]\text{[PF}_6]$  as supporting electrolyte. Electrochemical reduction in the presence of  
28 triethylammonium results in an irreversible response, but does not give rise to catalytic  $\text{H}_2$   
29 evolution, contrasting with the reactivity patterns observed in  $[\text{Cp}^*\text{Rh}]$  complexes bearing  
30 bipyridyl ligands with less electron-withdrawing substituents.

31 **Keywords:** rhodium; electrochemistry; paramagnetic; spectroelectrochemistry; catalysis.  
3233 

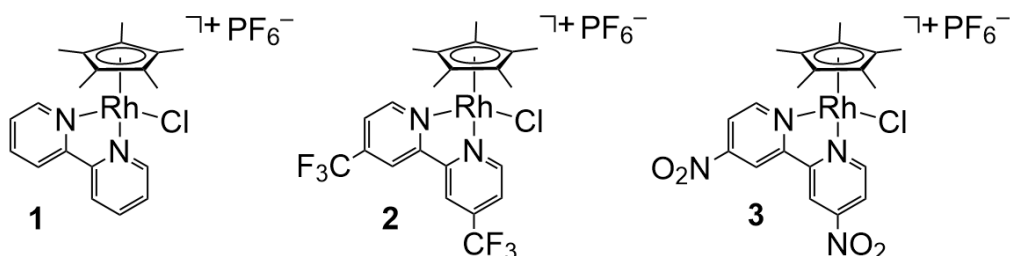
## 1. Introduction

34 The development of metal complexes capable of efficiently storing and transferring reducing  
35 equivalents attracts interest in a variety of contexts. Reduced metal complexes are key reaction  
36 intermediates in many transformations, including photoredox reactions enabled by reductive  
37 quenching pathways,<sup>1</sup> olefin polymerization or oligomerization,<sup>2</sup> and reactions involving  
38 concerted oxidative addition to transition metal complexes.<sup>3</sup> Reduced metal complexes also attract  
39 significant attention in the area of molecular electrocatalysis,<sup>4</sup> as several reduced intermediates are  
40 typically involved in multielectron redox cycles that generate fuels like  $\text{H}_2$  via  $\text{H}^+$  and  $\text{e}^-$  coupling.<sup>5,6</sup>  
41 In many of these cycles, however, the key metal complexes reduced by one or more  $\text{e}^-$  equivalents  
42 are not isolated or detected—instead, their involvement is inferred from the observed reactivity.

43  $[\text{Cp}^*\text{Rh}]$  complexes ( $\text{Cp}^*$  = pentamethylcyclopentadienyl) are one class of catalysts for  $\text{H}^+$  and  
44  $\text{e}^-$  coupling that are capable of generating  $\text{H}_2$  from water.<sup>7,8</sup> These catalysts are supported by

45 bidentate chelating ligands, such as 2,2'-bipyridyl (bpy, as in complex **1**) and its substituted  
 46 derivatives.<sup>9</sup>  $[\text{Cp}^*]$  and diimine ligands (like bpy) are readily installed through straightforward  
 47 synthetic chemistry onto the rhodium center in these compounds,<sup>10,11</sup> and thus this system has been  
 48 popular for model studies of  $\text{H}_2$  generation<sup>12</sup> as well as applications in other areas.<sup>13</sup> In this work,  
 49 two-electron reduction of the rhodium(III) precatalyst in the presence of a suitably strong acid  
 50 results in quantitative formation of  $\text{H}_2$  and regeneration of the starting rhodium(III) complexes.<sup>9</sup>  
 51 However, in chemistry that is distinctive for this family of catalysts, the putative rhodium(II)  
 52 intermediate generated by the initial  $1\text{e}^-$  reduction of a given precatalyst does not result in a stable  
 53 intermediate. In chemical work, treatment of  $\text{Rh}^{\text{III}}$  with 1 equiv. of reducing agent results in  
 54 disproportionation of two transient  $\text{Rh}^{\text{II}}$  complexes to yield 0.5 equiv. each of  $\text{Rh}^{\text{I}}$  and  $\text{Rh}^{\text{III}}$ .<sup>8</sup> In  
 55 electrochemical work, a so-called ECE-type event occurs at the electrode: a single reductive wave is  
 56 observed by cyclic voltammetry, corresponding to the first reduction of  $\text{Rh}^{\text{III}}$  (E), followed by a fast  
 57 chemical reaction step (C), and then immediate transfer of a second electron (E') to reduce  $\text{Rh}^{\text{II}}$  to  
 58  $\text{Rh}^{\text{I}}$ .<sup>14</sup> Thus,  $\text{Rh}^{\text{I}}$  is very quickly generated following formation of  $\text{Rh}^{\text{II}}$ , because the  $E(\text{Rh}^{\text{II}}/\text{Rh}^{\text{I}})$  is  
 59 more positive than  $E(\text{Rh}^{\text{III}}/\text{Rh}^{\text{II}})$ . These two-electron events obscure the routine measurement of the  
 60 individual one-electron reduction events involved in this chemistry.<sup>15,16</sup>

61



62

63

64

Chart 1.  $[\text{Cp}^*\text{Rh}]$  complexes discussed in this study.

65 The energy conversion efficiency of these  $[\text{Cp}^*\text{Rh}]$  catalysts is closely tied to the potentials of  
 66 the individual reduction events,<sup>17,18</sup> but only a limited level of control of these parameters has been  
 67 demonstrated to date. Moreover, the use of redox-active bpy ligands (and other diimines) in these  
 68 complexes has attracted significant attention.<sup>19,20,21</sup> Understanding the nature of the observed  
 69 reductions is key, as these  $[\text{Cp}^*\text{Rh}]$  complexes bearing diimine ligands undergo unique  
 70  $[\text{Cp}^*]$ -centered protonations<sup>22,23</sup> during catalysis to generate  $[\text{Cp}^*\text{H}]$  complexes<sup>24</sup> that are active for  
 71  $\text{H}_2$  evolution. Our group recently showed<sup>9</sup> that installation of electron-withdrawing trifluoromethyl  
 72 groups at the 4 and 4' positions of the bpy ligand (as in **2**) results in a previously unobserved  
 73 catalytic pathway involving reduction of the 4,4'-bis(trifluoromethyl)-2,2'-bipyridyl ligand on  
 74  $[(\text{Cp}^*\text{H})\text{Rh}^{\text{I}}]$  species, followed by  $\text{H}_2$  evolution. We have also found that  $[\text{Cp}^*\text{Rh}]$  complexes bearing  
 75 bidentate diphosphine<sup>25</sup> or hybrid phosphine-quinoline ligands<sup>26</sup> are not capable of similar  
 76 catalysis. Thus, although the role of supporting bidentate ligand structure in formation of  $[\text{Cp}^*\text{H}]$   
 77 intermediates is not yet clear, it is of high interest considering the new reactivity manifolds that  
 78 may be accessible with  $[\text{Cp}^*\text{H}]$  complexes.<sup>27,28</sup>

79 As use of 4,4'-bis(trifluoromethyl)-2,2'-bipyridyl enables observation of a new catalytic  
 80 pathway with **2**,<sup>9</sup> we became interested in the electrochemical behavior engendered by use of the  
 81 4,4'-dinitro-2,2'-bipyridyl (dnbpy) ligand, which features rather electron-withdrawing nitro groups  
 82 ( $-\text{NO}_2$ ). In considering use of the dnbpy ligand, it is useful to note the Hammett parameter ( $\sigma$ )  
 83 values associated with the hydrogen ( $-\text{H}$ ), trifluoromethyl ( $-\text{CF}_3$ ), and nitro functionalities ( $-\text{NO}_2$ ).  
 84 Specifically, these values are 0, 0.65, and 1.27, respectively.<sup>29</sup> Thus, in terms of the effects  
 85 engendered by substituents at the 4 and 4' positions on electronic properties, moving from  $-\text{CF}_3$  to  
 86  $-\text{NO}_2$  represents a similarly significant difference as moving from  $-\text{H}$  to  $-\text{CF}_3$ .

87 We were pleased to find that Lütz and co-workers previously reported preparation of  
 88  $[\text{Cp}^*\text{Rh}(\text{dnbpy})\text{Cl}]\text{Cl}$ ,<sup>30</sup> and that  $[\text{Cp}^*\text{Ir}]$  complexes bearing dnbpy have been known for some  
 89 years.<sup>31,32,33</sup> Moreover, dnbpy<sup>34,35,36</sup> and other nitrated polypyridyls<sup>37,38</sup> have been explored as  
 90 ligands to rhodium in other frameworks. We were especially intrigued to read that Lütz and

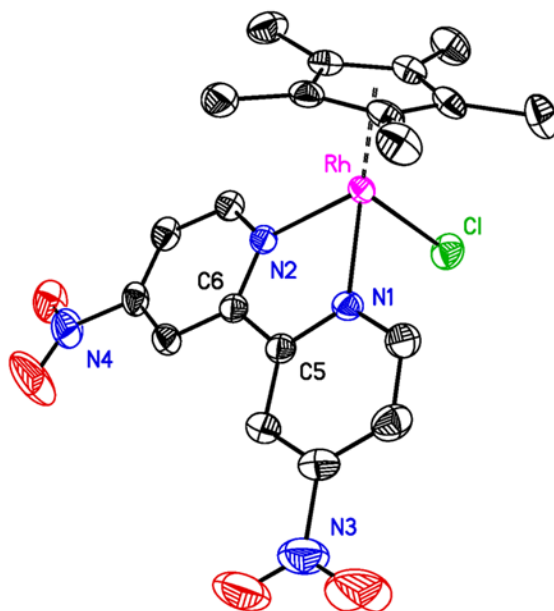
91 co-workers found that  $[\text{Cp}^*\text{Rh}(\text{dnbpy})\text{Cl}]\text{Cl}$  did not undergo electrochemical reduction in their  
92 hands down to  $-1$  V vs. Ag/AgCl in aqueous electrolyte.<sup>30</sup> However, in their report,  
93  $[\text{Cp}^*\text{Rh}(\text{dnbpy})\text{Cl}]\text{Cl}$  was prepared for use in a high-throughput, robotic electrochemical system,<sup>30</sup>  
94 rather than fully characterized with proof of homogeneity and bulk composition from synthetic  
95 work. Moreover, the electrochemical studies were carried out in aqueous electrolyte, rather than the  
96 organic electrolytes common in studies involving organometallic compounds.

97 Here, we now report the isolation, full characterization, and electrochemical studies of  
98  $[\text{Cp}^*\text{Rh}(\text{dnbpy})\text{Cl}]\text{PF}_6$  (3). We find that use of dnbpy engenders unique electrochemical properties  
99 in organic solvent-based electrolytes, as 3 undergoes three quasi-reversible one-electron reduction  
100 events and an additional, one-electron reduction event that is irreversible. The first, one-electron  
101 reduced product of 3 can be generated chemically and isolated, and spectroscopic work confirms  
102 that the first electron transferred is stored in orbitals primarily associated with the dnbpy ligand.  
103 Spectroelectrochemical studies reveal the clean interconversion of 3 and its reduction products, as  
104 isosbestic behavior is observed during multistep polarization experiments. Addition of acid in the  
105 form of triethylammonium bromide ( $\text{pK}_a \approx 19$  in MeCN<sup>39</sup>) does not result in generation of  
106 diamagnetic  $[\text{Cp}^*\text{H}]$  complexes or hydrides, and does not lead to catalytic activity toward  $\text{H}_2$   
107 evolution. These results are discussed in the context of understanding and guiding the order and  
108 energetics of  $e^-$  and  $\text{H}^+$  delivery to complexes assembled with the  $[\text{Cp}^*\text{Rh}]$  fragment.

## 109 2. Results

110 In order to study the properties of dnbpy complexes containing the  $[\text{Cp}^*\text{Rh}]$  fragment, we  
111 targeted synthesis of  $[\text{Cp}^*\text{Rh}(\text{dnbpy})\text{Cl}]\text{PF}_6$  (3). We have encountered cleaner reactivity of the  
112  $[\text{Cp}^*\text{RhCl}_2]_2$  precursor<sup>11</sup> upon use of silver reagents to remove one equivalent of chloride from each  
113 rhodium center, motivating preparation of the hexafluorophosphate salt 3.<sup>40,41</sup> We first synthesized  
114 dnbpy with literature methods, routinely obtaining an overall yield of ca. 50%.<sup>42,43,44</sup> 3 was then  
115 prepared in tetrahydrofuran (THF) by addition of 2 equiv. of dnbpy to  $[\text{Cp}^*\text{RhCl}_2]_2$ , followed by  
116 addition of 2 equiv. of  $\text{AgPF}_6$ , resulting in formation of the rhodium(III) complex 3 in moderate 44%  
117 yield (See Experimental Section and SI, Figures S1-S4, S6, S7 for characterization data).

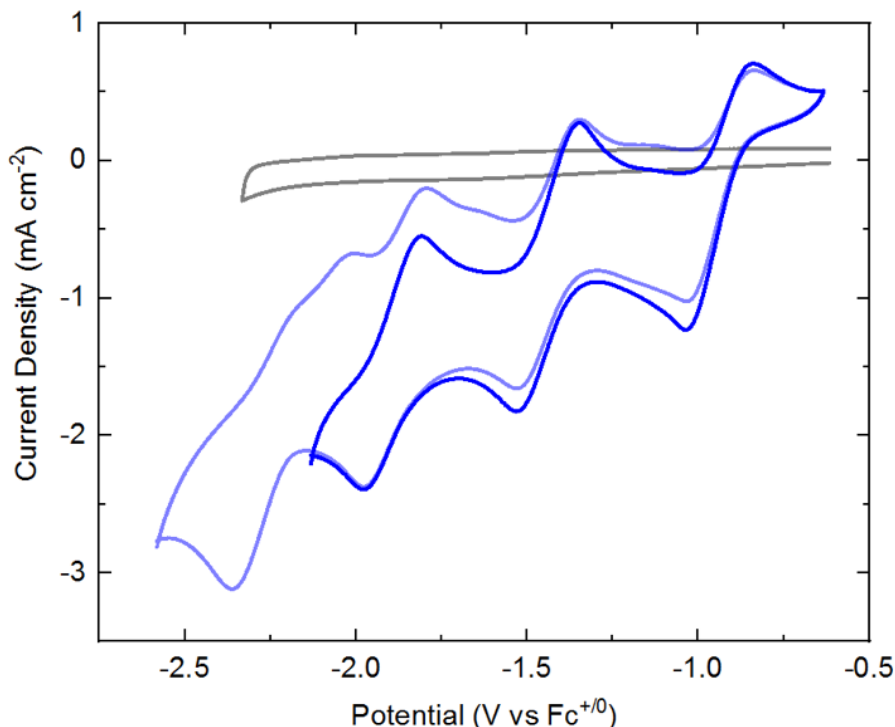
118 Vapor diffusion of diethyl ether into a concentrated acetonitrile (MeCN) solution of 3 yielded  
119 orange crystals suitable for single-crystal X-ray diffraction (XRD) studies. The geometry at the  
120 rhodium center is pseudo-octahedral, with a first coordination sphere around the metal center  
121 containing  $[\eta^5\text{-Cp}^*]$ ,  $[\kappa^2\text{-dnbpy}]$ , and a bound chloride anion (see Figure 1). The geometry and  
122 metal-ligand distances do not differ significantly from other structures of  $[\text{Cp}^*\text{Rh}^{\text{III}}]$  complexes  
123 containing 4,4'-disubstituted-2,2'-bipyridyl ligands.<sup>9</sup> However, only a limited number of XRD  
124 datasets are available in the Cambridge Structural Database for metal complexes of dnbpy, and our  
125 structure of 3 is the first structure obtained with rhodium.<sup>45</sup> In the structure of 3, as in most other of  
126 structures containing dnbpy, the  $(\text{NO}_2)$  groups are approximately co-planar with their partnered  
127 pyridine rings. In fact, of the seven total structures of dnbpy itself<sup>46</sup> or those containing dnbpy,<sup>47</sup>  
128 only one of these<sup>47b</sup> has a  $\text{O}-\text{N}-\text{C}-\text{C}$  torsion angle greater than  $13^\circ$ . The observed co-planarity of the  
129  $\text{NO}_2$  groups and the pyridine rings suggests that there is likely strong electronic communication  
130 between these substituents and the  $\pi$  system of bipyridine. Therefore, we turned to electrochemical  
131 methods to establish the influence of the nitro groups on the electrochemical properties of the metal  
132 complex.



133  
 134 **Figure 1.** Solid-state structure (XRD) of **3**. H atoms,  $\text{PF}_6^-$  counteranion, and one co-crystallized  
 135 MeCN molecule omitted for clarity. Displacement ellipsoids are shown at 50% probability.  
 136

137 Cyclic voltammograms (CV) of **3** (ca. 1 mM) were collected in THF solution containing 0.1 M  
 138 tetrabutylammonium hexafluorophosphate ( $[\text{NBu}_4]\text{[PF}_6]$ ) as supporting electrolyte. Beginning at  
 139 oxidizing potentials, **3** displays a manifold of four reduction events (see Figure 2) that onset around  
 140  $-1$  V versus the ferrocenium/ferrocene couple (denoted hereafter as  $\text{Fc}^{+0}$ ). The key parameters  
 141 associated with each of these four reduction events are summarized in Table 1. If the switching  
 142 potential for the return anodic sweep is set at  $-2.2$  V, the first three reduction events appear to be  
 143 quasi-reversible with well-defined, clean return anodic waves. However, if the switching potential  
 144 is set at a more negative value of  $-2.6$  V, the fourth reduction wave is clearly visible. This fourth  
 145 reduction, however, is not accompanied by a clean return oxidation wave, suggesting that one or  
 146 more significant chemical reactions may follow injection of a fourth electron into the rhodium  
 147 complex. Interrogation of the scan rate dependence of the both the cathodic and anodic peak  
 148 currents for the first three observed redox processes reveals a square-root dependence (see SI,  
 149 Figures S13-S15). This indicates that all the oxidized and reduced forms of the complex undergoing  
 150 reduction and oxidation are freely diffusional in solution and homogeneous.

151 We also carried out cyclic voltammetry of **3** in acetonitrile electrolyte, and consistently  
 152 observed a similar manifold of reduction events (see SI, Figure S10). Specifically, three  
 153 quasi-reversible reductions are followed by a virtually irreversible reduction.<sup>48</sup> However, we  
 154 conducted most of our studies in THF electrolyte, as the complex typically yielded a better response  
 155 under these conditions.



156  
 157 **Figure 2.** Cyclic voltammograms of **3**. Scan rate: 100 mV/s. Dark blue line: Cathodic sweep from ca.  
 158 –0.6 V to a switching potential of –2.2 V and returning to –0.6 V. Light blue line: Cathodic sweep  
 159 from ca. –0.6 V to a switching potential of –2.6 V and returning to –0.6 V. Gray line: electrolyte-only  
 160 blank. Conditions:  $[3] \approx 1 \times 10^{-3}$  M; electrolyte: 0.1 M  $[\text{NBu}_4][\text{PF}_6]$  in THF.

161  
 162 **Table 1.** Cyclic voltammetry data for **3**. Conditions:  $[3] = 10^{-3}$  M; scan rate: 100 mV/s; electrolyte: 0.1  
 163 M  $[\text{NBu}_4][\text{PF}_6]$  in THF.

Redox event	$E_{1/2}$ (V)	$\Delta E_p$ (V)	$E_{p,c}$ (V)	$E_{p,a}$ (V)
A	–0.94	0.20	–1.04	–0.84
B	–1.44	0.18	–1.53	–1.35
C	–1.89	0.17	–1.98	–1.81
D	–	–	–2.36	–

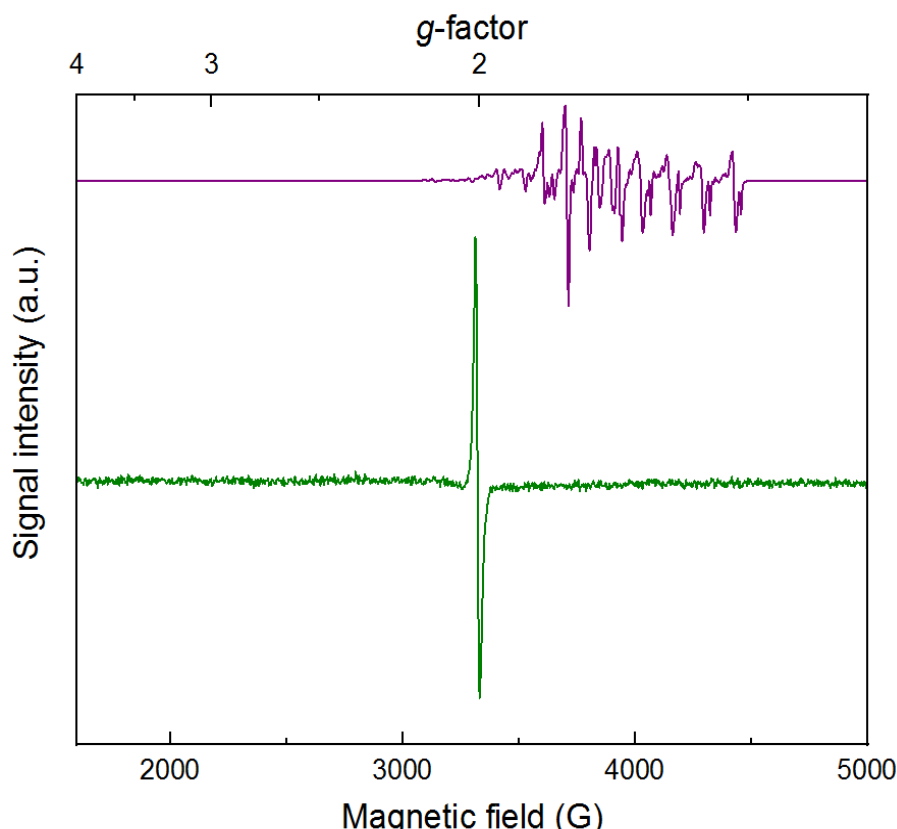
164  
 165 In the cyclic voltammetry shown in Figure 2, the peak heights of the reduction processes  
 166 appear to be similar, suggesting that the same number of electrons are transferred during each  
 167 event. However, as the individual reduction events are relatively closely spaced, estimation of the  
 168 appropriate background-corrected peak heights could be challenging. Therefore, differential pulse  
 169 voltammetry (DPV) was carried out to quantitatively examine the number of electrons transferred  
 170 in each event. For this determination, we prepared a solution containing a 1:1 mixture of ferrocene  
 171 ( $\text{Cp}_2\text{Fe}$ ) and **3** in THF containing 0.1 M  $[\text{NBu}_4][\text{PF}_6]$  supporting electrolyte and collected a  
 172 differential pulse voltammogram from +0.5 V to –2.6 V (see SI, Figure S12). In addition to the  
 173 one-electron process corresponding to the  $\text{Fe}^{\text{III}}/\text{Fe}^{\text{II}}$  couple of ferrocene, we observe four closely  
 174 spaced and reasonably well resolved processes over a range similar to that seen for **3** in cyclic  
 175 voltammetry. The areas of the four processes measured for **3** and that of  $\text{Cp}_2\text{Fe}$  were fit to Gaussian  
 176 profiles, and comparison of the peak areas to that of the internal ferrocene standard confirms that  
 177 one electron is indeed transferred in each event (see SI, Table S3 for peak area ratios).

178 The electrochemical response of complex **3** sharply contrasts with the behavior commonly  
 179 encountered for other  $[\text{Cp}^*\text{Rh}^{\text{III}}]$  complexes. Most other chloride-bound complexes in this family  
 180 containing other diimine,<sup>7,9,12,13</sup> diphosphine,<sup>8,25</sup> or hybrid phosphine-monoimine ligands,<sup>26</sup> undergo  
 181 a net two-electron reduction that appears as a single redox process in cyclic voltammetry  
 182 experiments. As described in the Introduction, this ECE-type electrochemical response implicates

183 that a chemical reaction follows the initial reduction of the metal complex and leads to formation of  
184 a species that undergoes immediate transfer of a second electron.<sup>14</sup> Disentangling the nature of the  
185 elementary steps in this chemistry is of high interest, as the resulting 2e<sup>-</sup>-reduced complexes often  
186 undergo subsequent reactivity with protons. Notably, our recent work examining the case of a  
187 [Cp<sup>\*</sup>Rh] complex bearing the hybrid 8-(diphenylphosphino)quinoline (PQN) ligand suggests that  
188 the first reduction of [Cp<sup>\*</sup>Rh<sup>III</sup>(PQN)Cl]PF<sub>6</sub> is rhodium-centered, and leads to ejection of the  
189 chloride ligand at the Rh<sup>II</sup> oxidation state.<sup>26</sup> The electrochemical behavior of the [Cp<sup>\*</sup>Rh] complex  
190 supported by the dimethyldipyridylmethane (Me<sub>2</sub>dpma) ligand is also consistent with initial  
191 metal-centered reduction.<sup>40</sup>

192 Therefore, to investigate the nature of the first reduction of **3**, we targeted preparation of the  
193 singly reduced product. In accord with the clean, one-electron reduction of **3** observed by cyclic  
194 voltammetry, treatment of a THF suspension of **3** with cobaltocene ( $E^{\circ} \approx -1.3$  V,<sup>49</sup> 2 equiv.) results  
195 in an immediate color change from bright yellow to a deep shade of forest green. Following stirring  
196 for 10 minutes and subsequent removal of all volatiles under vacuum, the reduction product **4** was  
197 extracted with THF and isolated as a dark green solid. Characterization of **4** by <sup>1</sup>H NMR (Figure S5)  
198 reveals a loss of all resonances associated with **3**, including those of the [ $\kappa^2$ -dnbpy] ligand in the  
199 aromatic region and that associated with [ $\eta^5$ -Cp<sup>\*</sup>] in the aliphatic region. The disappearance of  
200 these resonances and lack of new peaks associated with diamagnetic material is consistent with  
201 generation of a paramagnetic complex, as would be expected for a 1e<sup>-</sup> reduction of **3** as observed in  
202 cyclic voltammetry. A small impurity of [Cp<sub>2</sub>Co]<sup>+</sup> ( $\delta = 5.66$  ppm) is observed in NMR spectra of  
203 isolated samples from the reduction of **3**, but could not be removed due to the similar solubility  
204 profiles of **4** and cobaltocenium.

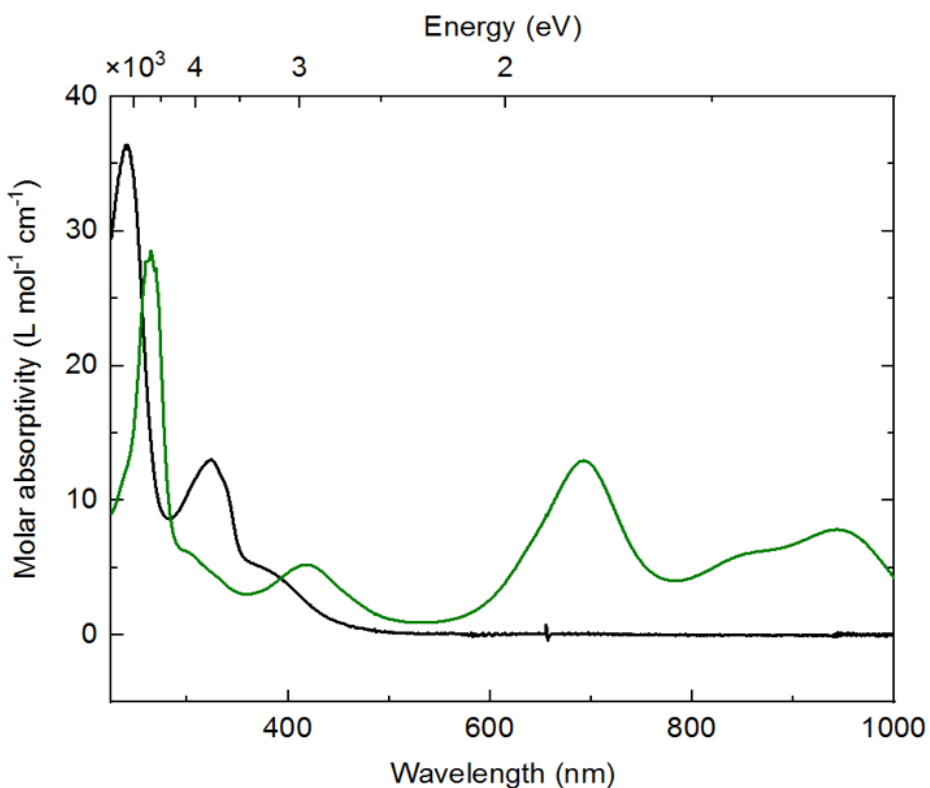
205 To further characterize **4**, we turned to electron paramagnetic resonance spectroscopy. Prior to  
206 reduction, **3** is a low-spin rhodium(III) complex with a  $d^6$  configuration and  $S = 0$ . The cobalt(II)  
207 reductant (Cp<sub>2</sub>Co) used to generate **4** has a  $d^7$  configuration and is a  $S = 1/2$  species, displaying the  
208 distinctive spectrum (consistent with literature) shown as the purple line in Figure 3. This spectrum  
209 displays hyperfine coupling to the  $I = 7/2$  cobalt nucleus. In contrast, the spectrum of **4** isolated as  
210 described above reveals a relatively narrow and isotropic signal with a center crossing point at  $g =$   
211 2.006 ( $H = 3341$  G). Although **4** could be considered to be a formal rhodium(II) species, the sharp  
212 and isotropic spectrum is instead consistent with an organic radical—in this case, predominant  
213 localization of unpaired electron density on the dnbpy ligand. Thus, **4** can be most appropriately  
214 considered as a rhodium(III) complex with a bound dnbpy<sup>•-</sup>. Retention of this ligand radical in the  
215 first coordination sphere of the rhodium center is consistent with both the quasi-reversible CV  
216 studies (vide supra) and spectroelectrochemical work that confirms the chemically reversible  
217 interconversion of **3** and **4** (vide infra) on the seconds to minutes timescale. Moreover, the lack of  
218 resolved hyperfine coupling to the  $I = 1/2$  <sup>103</sup>Rh nucleus (100% abundance) in **4** corroborates  
219 assignment of the reduced metal species as having unpaired electron density that is localized  
220 primarily on dnbpy. Notably, the trace impurity of [Cp<sub>2</sub>Co]<sup>+</sup> present in samples of isolated **4** does  
221 not contribute to the EPR spectrum shown in Figure 3, as [Cp<sub>2</sub>Co]<sup>+</sup> is an  $S = 0$  low-spin cobalt(III)  
222 complex.



223  
 224 **Figure 3.** X-band CW EPR spectrum of **4** (green line) and cobaltocene (purple line). Conditions:  $T =$   
 225 10 K; modulation amplitude = 2.0 G; time constant = 20.5 ms;  $[4] = 10^{-3}$  M.  
 226

227 Few examples of formal rhodium(II) complexes have been observed by EPR.<sup>50</sup> Localization of  
 228 unpaired electron density in orbitals with increased Rh(II) character would be expected to result in  
 229 a significantly more anisotropic spectrum than that observed for **4**, with larger g-value shifts and  
 230 resolved hyperfine coupling to the metal nucleus. The experimental data for **4** compare well with  
 231 data that we have recently obtained on  $[\text{Cp}^*\text{Rh}(\text{bpy}^{\bullet-})\text{Me}]^0$  and  $[\text{Cp}^*\text{Ir}(\text{bpy}^{\bullet-})\text{Me}]^0$  compounds.<sup>41</sup>  
 232 Specifically, these methyl complexes display narrow rhombic spectra centered near  $g \approx 2.0$ . This  
 233 greater rhombicity arises from hyperfine couplings to the  $I = 1/2$  Rh<sup>III</sup> and  $I = 3/2$  Ir<sup>III</sup> centers in these  
 234 compounds, contrasting with the case of virtually ligand-centered **4**. Thus, we conclude that the  
 235 unpaired electron density on dnbpy<sup>•-</sup> is contained in molecular orbitals with very little character  
 236 arising from rhodium, a phenomenon likely driven by the presence of the strongly  
 237 electron-withdrawing nitro groups on dnbpy.  
 238

239 To gain further insight into the dnbpy-localization of electron density arising from the first  
 240 reduction of **3**, we turned to electronic absorption spectroscopy (see Figure 4 and SI, Figure S8). The  
 241 spectrum of **3** is unremarkable and displays features consistent with most rhodium(III) complexes;  
 242 **3** is a yellow solid, and the UV-visible absorption spectrum reflects this with a relatively intense (ca.  
 243  $5000 \text{ M}^{-1} \text{ cm}^{-1}$ ) band trailing into the visible around 400 nm. Isolated **4** displays a very different  
 244 profile, with distinctive new features in the visible-NIR region ( $\lambda_{\text{max}}$  values at 694 nm, 860 nm, and  
 245 945 nm with molar absorptivities of 13000, 6100, and  $7800 \text{ M}^{-1} \text{ cm}^{-1}$ , respectively). Consistent with  
 246 the observed forest-green color of **4**, a weaker absorption band is retained at lower wavelength (420  
 247 nm,  $5200 \text{ M}^{-1} \text{ cm}^{-1}$ ) and thus transmits predominantly green light between these bands. The  
 248 absorption bands in the 800-1000 nm range are similar to examples of both free bpy<sup>•-</sup> and metal  
 249 complexes ligated by [bpy<sup>•-</sup>].<sup>51,52</sup> Analogous data is not available from prior work for dnbpy<sup>•-</sup>,  
 250 although similar features are measured for the doubly reduced form of complex **2**, which possesses  
 251 significant reduced-ligand character.<sup>9</sup> Thus, both EPR and electronic absorption data are consistent  
 with assignment of dnbpy-centered reduction in **4**.

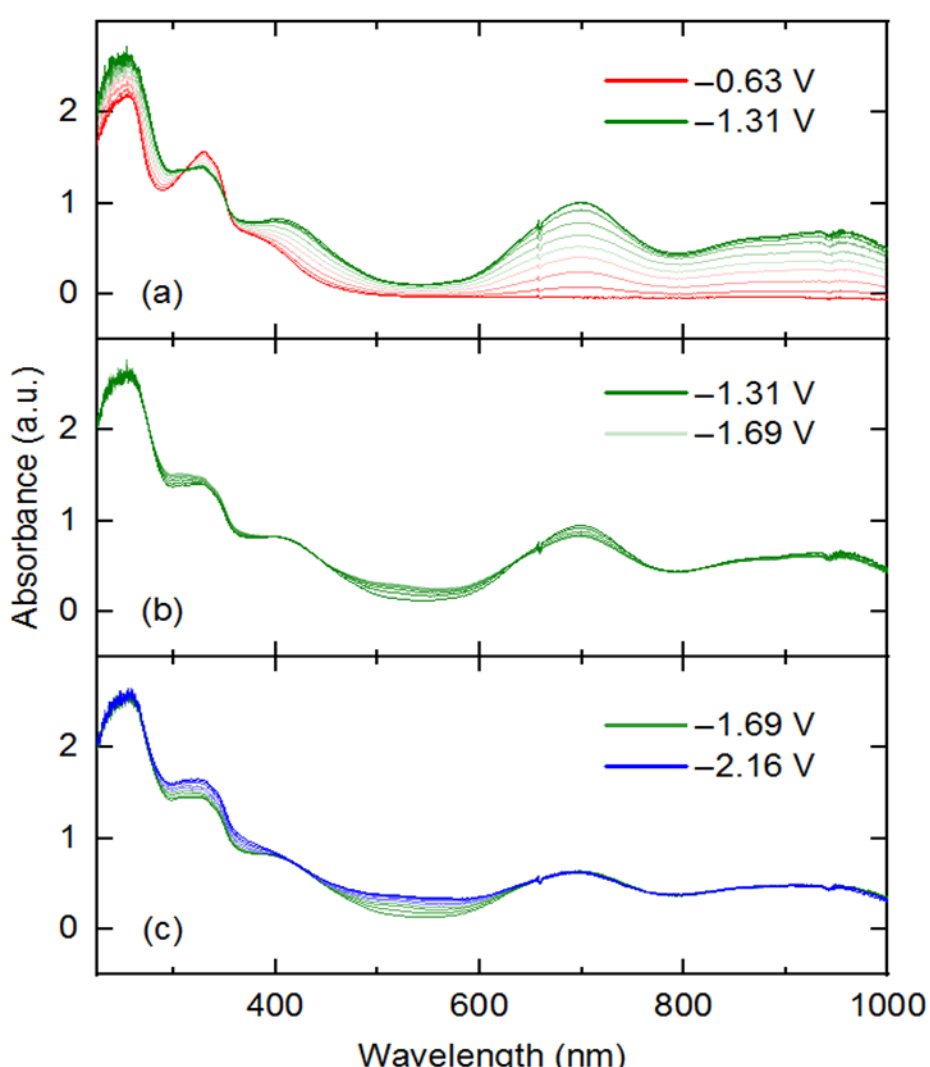


252  
 253 **Figure 4.** Electronic absorption spectra of **3** (black line) and **4** (green line). Conditions:  $[3] \approx [4] \approx$   
 254  $10^{-5}$ ; solvent: tetrahydrofuran.

255 Metal-centered reduction of  $[\text{Cp}^*\text{Rh}^{\text{III}}]$  complexes is associated with ejection of monodentate  
 256 ligands such as chloride from the first coordination sphere. This phenomenon is driven by  
 257 formation of transient, 19e<sup>-</sup> Rh<sup>II</sup> intermediates upon reduction that release the monodentate ligand  
 258 to form more stable 17e<sup>-</sup> species.<sup>26</sup> The assignment of ligand-centered reduction of **3** thus prompted  
 259 us to explore whether analogous reactivity takes place here. To test this, we performed cyclic  
 260 voltammetry on **3** in acetonitrile containing 0.1 M  $[\text{NBu}_4]\text{Cl}$  as supporting electrolyte. The first  
 261 reduction of **3** remains unchanged from the case of  $[\text{NBu}_4]\text{PF}_6$ , showing a quasi-reversible  
 262 appearance. However, the appearance of the second reduction of **3** (or reduction of **4**) is different,  
 263 showing two peaks on the cathodic sweep ( $\Delta E \approx 175$  mV) and a single peak on the anodic sweep  
 264 (see SI, Figure S11). This is consistent with the formation of both the cationic solvento complex  
 265  $[\text{Cp}^*\text{Rh}(\text{dnbpy}^{\bullet-})(\text{NCMe})]\text{PF}_6$  and a neutral chloride complex  $\text{Cp}^*\text{Rh}(\text{dnbpy}^{\bullet-})\text{Cl}$  following the first  
 266 reduction, when the electrolyte contains a 100-fold excess of chloride. Thus, under conditions where  
 267 chloride is not found in excess (Figure 2), we propose that reduction of **3** leads exclusively to  
 268 generation of the 18e<sup>-</sup>, cationic  $[\text{Cp}^*\text{Rh}(\text{dnbpy}^{\bullet-})(\text{NCMe})]\text{PF}_6$  complex. Consistent with this  
 269 significant coupled chemical reaction, the peak-to-peak separation ( $\Delta E_p \approx 200$  mV in THF, 90 mV in  
 270 MeCN) associated with reduction of **3** to **4** in  $[\text{NBu}_4]\text{PF}_6$  is significantly larger than those  
 271 associated with the following two reductions (180, 170 mV in THF; 70, 70 mV in MeCN) (see Table 1  
 272 and Table S1 in SI). Completing our proposed model for the electrochemistry, reduction of **4** leads  
 273 to a single product, on the basis of the single anodic wave observed at  $-1.35$  V in THF (Figure 2) and  
 274  $-1.19$  V in MeCN (see SI, Figure S10). As this species is rather electron-rich, we speculate that the  
 275 reduction of **4** produces  $[\text{Cp}^*\text{Rh}(\text{dnbpy})]^0$ ; however, further assignments regarding this compound  
 276 are beyond the scope of this study.

277 To gain further insight into the reductions of **3** that are readily accessible via electrochemical  
 278 methods, we turned to UV-visible spectroelectrochemistry. We took the approach of *in situ*  
 279 generation and detection of **4** and other reduced forms of **3** by use of a short-pathlength cuvette cell  
 280 placed in the beam path of a UV-visible spectrophotometer for real-time data collection during  
 281 working electrode polarization. With the working electrode polarized at  $-0.63$  V vs.  $\text{Fc}^{+0}$ , the  
 282 spectrum of **3** contained in the cell (electrolyte: 0.1 M  $[\text{NBu}_4]\text{PF}_6$  in THF) is virtually identical to

283 that of **3** in pure THF free from supporting electrolyte. However, upon polarization at  $-1.31$  V, the  
 284 spectrum changes dramatically (Figure 5, panel a), with new features appearing that correspond to  
 285 those of rhodium(III) bound to reduced dnbpy $^{+}$ . Notably, isosbestic points were measured at 312  
 286 and 352 nm (Figure S22), consistent with clean conversion of **3** to **4** in THF solution under the  
 287 spectroelectrochemical conditions. However, close comparison of the spectroelectrochemical data  
 288 (collected in THF electrolyte containing  $0.1$  M  $[\text{NBu}_4]\text{[PF}_6]$ ) and the earlier UV-visible data collected  
 289 on **4** (in pure THF) reveals that the  $\lambda_{\text{max}}$  values are slightly shifted in the two cases (417 vs. 418, 699  
 290 vs. 693, 865 vs. 860, 946 vs. 944 nm, respectively) (see SI, Figure S28). These minor differences are  
 291 consistent with ligand exchange of chloride in favor of THF, facilitated by  $0.1$  M  $[\text{NBu}_4]\text{[PF}_6]$ , as  
 292 similar spectral changes accompany exchange of halide ligands for coordinated solvent (e.g.,  
 293 MeCN) in other rhodium(III) complexes.<sup>21,26</sup>  
 294



295  
 296 **Figure 5.** UV-visible-NIR absorption spectra obtained during spectroelectrochemical studies as  
 297 described in the main text. Initial potentials for each experiment were  $-0.63$  V (panel a),  $-1.31$  V  
 298 (panel b), and  $-1.69$  V (panel c). Final potentials were  $-1.31$  V (panel a),  $-1.69$  V (panel b), and  $-2.16$   
 299 V (panel c). Final potential was held until no spectral changes were reached, indicating full  
 300 conversion of the thin-layer region to the desired form of the complex.  
 301

302 To confirm the apparent chemical reversibility observed in cyclic voltammetry for  
 303 transformation of **3** to **4** (Figure 2) and **4** to **3** (see SI, Figure S16), an experiment was also carried out  
 304 with an initial potential of  $-1.31$  V and final potential of  $-0.63$  V in an electrolyte solution prepared  
 305 with **4** (see SI, Figure S26). In this experiment, the evolution of the spectral features detected in the

306 experiment shown in Figure 1a were essentially reversed. This is consistent with clean regeneration  
307 of complex **3** from **4** upon electrochemical re-oxidation (isosbestic points at 312 and 352 nm).

308 Further potential excursions show spectral changes associated with the further reductions of **3**.  
309 A potential jump from  $-1.31$  to  $-1.69$  V results in fairly minor changes to the UV-visible spectrum  
310 (Figure 5b). Clear isosbestic points were observed at 437, 638, and 800 nm for this reduction event,  
311 corresponding to increased spectral absorption toward the blue region (522 nm) and slightly  
312 attenuated absorption intensity (peak at 699 nm) toward the longer wavelengths. A further  
313 potential excursion to  $-2.16$  V (Figure 5c) results in further increases in absorption toward shorter  
314 wavelengths (325 and 522 nm), and virtually no changes in absorption at the longer wavelengths  
315 (isosbestic point at 420 nm). Based on the isosbestic behavior, we confirm the interconversion of  
316 single species implied by the electrochemical studies carried out in  $[\text{NBu}_4][\text{PF}_6]$ .<sup>25,8</sup>

317 However, final potential excursion to  $-2.56$  V results in non-isosbestic spectral evolution  
318 (Figures 5c and SI, Figure S25), suggesting formation of multiple speciation products or  
319 decomposition of the four-electron reduced species generated from **3**. This behavior is consistent  
320 with the irreversible reduction observed at  $-2.36$  V in the voltammetry of **3** and confirms that the  
321 quadruply reduced form of **3** is unstable under electrochemical and spectroelectrochemical  
322 conditions. Study of the electronic structure of these further reduced intermediates is deserving of  
323 future work, especially focusing on the localization of each reduction (metal, ligand, both) and  
324 coordination geometry of rhodium (presence or absence of bound chloride or solvent).  
325 Computational approaches could be of great use here, as well as further spectroscopic and  
326 synthetic/structural investigations.

327 As reduction of most  $[\text{Cp}^*\text{Rh}]$  complexes bearing diimine-type ligands in the presence of acid  
328 can give rise to catalytic  $\text{H}_2$  production, we examined electrochemical reduction of **3** in the presence  
329 of acid to check for formation of  $\text{H}_2$  (as has been measured for both **1** and **2**). We conducted these  
330 studies with **3** in MeCN electrolyte (in order to rely on the well-defined  $\text{pK}_a$  scale that is available in  
331 this solvent).<sup>18,39</sup> Addition of 1 atm of  $\text{H}_2$  gas to the headspace of the electrochemical cell results in  
332 no major changes to the voltammetric profile, confirming that **3** does not readily serve as a catalyst  
333 for  $\text{H}_2$  oxidation (see SI, Figure S17). However, addition of 15 equiv. of buffered  $\text{Et}_3\text{NH}^+/\text{Et}_3\text{N}$  results  
334 in a fully irreversible voltammetric profile, and a modest increase in current density across a broad  
335 potential range from  $-1$  V to around  $-2$  V (see SI, Figure S17). Beyond  $-2$  V, there is a significant  
336 enhancement in the current flowing in the voltammetry, although at these potentials similar current  
337 enhancement is also observed for a rhodium-free electrolyte solution containing only buffered acid.

338 Bulk electrolysis was then carried out to ascertain the fate of the reducing equivalents  
339 transferred to the solution under these acidic conditions. Electrolysis was carried out at  $-1.75$  V,  
340 prior to the onset of significant background currents, to reveal the behavior of the reduced metal  
341 complexes with acid. In a rhodium-free control experiment, 17.2 C of charge were passed through  
342 the electrochemical cell, and a fairly significant amount of  $\text{H}_2$  was generated corresponding to 87%  
343 Faradaic efficiency (product  $\text{H}_2$  measured by gas chromatography). The analogous electrolysis  
344 carried out with **3** (Figure S18) leads to passage of only 8.2 C of charge, corresponding to 1.95 e<sup>-</sup> per  
345 Rh center. A Faradaic yield of  $\text{H}_2$  of only 5% was measured by gas chromatography, confirming  
346 that **3** does not serve as an effective (pre)catalyst for  $\text{H}_2$  evolution under these conditions.

347 During electrolysis, the solution of **3** remains homogeneous, but turns a dark red color. To  
348 investigate, aliquots of the working solution were removed from the cell following electrolysis, the  
349 solvent removed *in vacuo*, and  $^1\text{H}$  NMR data collected in  $\text{CD}_3\text{CN}$  to ascertain the identity of  
350 products formed by reaction of reduced **3** with acid. The  $^1\text{H}$  NMR data reveal that several ( $\geq 3$ )  
351 diamagnetic dnbpy containing species are generated, based on the presence of multiple sets of  
352 dnbpy-like resonances in the aromatic region (see SI, Figure S19). However, no metal hydride  
353 signals were observable in the upfield region near  $-10$  ppm (Figure S20),<sup>25,26</sup> nor were the  
354 characteristic signals corresponding to formation of  $[\text{Cp}^*\text{H}]$  (e.g., a doublet near 0.5 ppm) detected  
355 (Figures S19b and S19c in SI).<sup>24</sup> Thus, we conclude that decomposition accompanies reduction and  
356 protonation of **3**, resulting in formation of multiple products but no  $\text{H}_2$ .

358 **3. Discussion**

359 The observation of four one-electron reduction events with complex **3** contrasts with the single  
360 two-electron, ECE-type reduction<sup>14</sup> events measured for most other diimine and diphosphine  
361 complexes of [Cp<sup>\*</sup>Rh].<sup>7,8,9,25,26</sup> Results from our laboratory suggest that the first reduction is rhodium  
362 metal-centered in most of these cases.<sup>40</sup> Thus, initial metal-centered reduction generates a transient  
363 19e<sup>-</sup> rhodium(II) complex that undergoes subsequent ligand dissociation (to a 17e<sup>-</sup> species) and  
364 further reduction. **3** circumvents this more common reactivity by undergoing a first,  
365 ligand-centered reduction that leads only to *exchange* of bound chloride or solvent. As a side note,  
366 we have recently chemically prepared an analogous formal rhodium(II) complex bearing a  
367 bis(pyridyl) ligand; this complex is a metal-centered radical that circumvents further reduction  
368 through use of the bis(pyridyl) ligand that enforces a six-membered metallocyclic ring.<sup>40</sup> Here, we  
369 conclude that inclusion of the easily reduced dnbpy ligand and retention of a monodentate ligand  
370 in **4** contribute to the ability of the complexes to undergo sequential, one-electron reductions.

371 Our formulation of **4** as a ligand-centered radical is consistent with prior work from  
372 Yellowlees's group<sup>53</sup> on the nature of reduced species formed by reduction of nitrated bpy  
373 complexes of Pt<sup>II</sup>. Specifically, their group found that the LUMO of Pt(dnbpy)Cl<sub>2</sub> is localized on the  
374 dnbpy ligand; on the basis of exhaustive EPR spectroelectrochemistry and computational studies,  
375 they further assigned the radical in Pt(dnbpy<sup>•</sup>)Cl<sub>2</sub> to be localized on a single 4-NO<sub>2</sub>-pyridyl ring.  
376 The Pt compounds in their study displayed rich hyperfine structure in EPR spectra, enabling this  
377 assignment. In our EPR data for **4**, however, no such fine structure is observable. Thus, further  
378 work is needed to distinguish details of the exact localization of unpaired electron density within  
379 the conjugated dnbpy system.

380 Cp<sup>\*</sup>Rh(bpy) undergoes reaction with protons to form [Cp<sup>\*</sup>H] species that are active  
381 intermediates in catalytic H<sub>2</sub> production.<sup>22,23</sup> Therefore, the observation of virtually no  
382 H<sub>2</sub>-generating reactivity of reduced forms of **3** with protons is interesting from the perspective of  
383 understanding the structure and bonding features that engender catalysis involving H-atom  
384 transfer<sup>24,25</sup> from [Cp<sup>\*</sup>Rh] complexes. In the chemistry of most [Cp<sup>\*</sup>Rh] complexes, apparently  
385 metal-centered reduction is followed by reactivity with protons to form either [Cp<sup>\*</sup>H] complexes<sup>24</sup>  
386 or stable rhodium(III) hydride species.<sup>25,26</sup> Based on electrochemical studies of **3** in the presence of  
387 Et<sub>3</sub>NH<sup>+</sup>, we conclude that one or more of the reduced forms of **3** undergo reaction with protons, but  
388 these do not lead to effective H<sub>2</sub> generation.

389 However, involvement in ligand orbitals in reduction events does not necessarily preclude  
390 proton reactivity in [Cp<sup>\*</sup>Rh] complexes; rather, our results suggest that the electron-donating and  
391 -withdrawing character of ligands on these frameworks must be carefully balanced to  
392 accommodate the intermediates that may arise during catalysis. This conclusion is well supported  
393 by the prior work implicating a delocalized HOMO across the metal and ligands in most  
394 Cp<sup>\*</sup>Rh(diimine) complexes, and the reactivity of the doubly reduced forms of **1** and **2** with protons  
395 towards hydrogen evolution.<sup>9</sup>

396 **4. Conclusions**

397 We have described the preparation, characterization, and electrochemical properties of  
398 [Cp<sup>\*</sup>Rh<sup>III</sup>(dnbpy)Cl]PF<sub>6</sub> (**3**). This complex displays four one-electron reduction events in organic  
399 electrolytes, contrasting with prior work on a similar complex that showed no reductions in  
400 aqueous electrolyte. Spectroscopic studies show that the singly reduced complex **4** generated from **3**  
401 is best formulated as [Cp<sup>\*</sup>Rh<sup>III</sup>(dnbpy<sup>•</sup>)(L)]<sup>+</sup> where L = chloride or solvent, depending upon the  
402 conditions of the experiment. Spectroelectrochemical studies suggest clean interconversion of the  
403 various reduced forms, as isosbestic behavior is obtained in the UV-visible spectra associated with  
404 controlled potential excursions. However, in contrast to other [Cp<sup>\*</sup>Rh] complexes bearing diimine  
405 ligands, electrochemical studies of **3** in the presence of excess Et<sub>3</sub>NH<sup>+</sup> show that reduction in the  
406 presence of this weak acid does not lead to H<sub>2</sub> production. Taken together, these studies show that  
407 [Cp<sup>\*</sup>Rh] complexes, and the reactions that they undergo upon electron transfer, are readily tunable

408 by judicious selection of supporting ancillary ligands. Our ongoing work is examining this strategy  
409 to harness the useful properties of this family of compounds.

## 410 5. Materials and Methods

### 411 5.1. General Considerations

412 All manipulations were carried out in dry N<sub>2</sub>-filled gloveboxes (Vacuum Atmospheres Co.,  
413 Hawthorne, CA) or under N<sub>2</sub> atmosphere using standard Schlenk techniques unless otherwise  
414 noted. All solvents were of commercial grade and dried over activated alumina using a PPT Glass  
415 Contour (Nashua, NH) solvent purification system prior to use, and were stored over molecular  
416 sieves. All chemicals were from major commercial suppliers and used as received after extensive  
417 drying. [Cp\*RhCl<sub>2</sub>]<sub>2</sub> was prepared according to the literature procedure.<sup>10</sup> The  
418 4,4'-dinitro-2,2'-bipyridyl ligand (dnbpy) was prepared with literature methods from  
419 2,2'-bipyridine (bpy).<sup>42,43,44</sup> Deuterated NMR solvents were purchased from Cambridge Isotope  
420 Laboratories; CD<sub>3</sub>CN was dried over molecular sieves. <sup>1</sup>H, <sup>13</sup>C, <sup>19</sup>F, and <sup>31</sup>P NMR spectra were  
421 collected on 400 or 500 MHz Bruker spectrometers and referenced to the residual protio-solvent  
422 signal in the case of <sup>1</sup>H and <sup>13</sup>C.<sup>54</sup> Heteronuclear NMR spectra were referenced to the appropriate  
423 external standard following the recommended scale based on ratios of absolute frequencies ( $\Xi$ ).<sup>55</sup>  
424 <sup>19</sup>F NMR spectra are reported relative to CCl<sub>3</sub>F, and <sup>31</sup>P NMR spectra are reported relative to H<sub>3</sub>PO<sub>4</sub>.  
425 Chemical shifts ( $\delta$ ) are reported in units of ppm and coupling constants ( $J$ ) are reported in Hz.  
426 Elemental analyses were performed by Midwest Microlab, Inc. (Indianapolis, IN).

427 Electronic absorption spectra were collected with an Ocean Optics Flame spectrometer or a  
428 Shimadzu 3600 UV-vis-NIR spectrometer, in 1-cm pathlength quartz cuvettes.

429 Continuous-wave electron paramagnetic resonance were collected at X-band with a Bruker  
430 EMX spectrometer using a high-sensitivity perpendicular-mode cavity (4119HS-W1). Temperature  
431 control was achieved with an Oxford ESR 900 flow-through cryostat.

### 432 5.2. X-ray crystallography

433 Single-crystal diffraction data were collected with a Bruker APEX-II CCD diffractometer. CCDC  
434 entry 1842459 contains the supplementary crystallographic data for compound 3. These data can be  
435 obtained free of charge via [www.ccdc.cam.ac.uk/data\\_request/cif](http://www.ccdc.cam.ac.uk/data_request/cif), or by emailing  
436 data\_request@ccdc.cam.ac.uk, or by contacting The Cambridge Crystallographic Data Centre, 12,  
437 Union Road, Cambridge CB2 1EZ, UK; fax: +44 1223 336033.

### 438 5.3. Electrochemistry

439 Electrochemical experiments were performed in a N<sub>2</sub>-filled glovebox in dry, degassed THF or  
440 MeCN. 0.10 M tetra(n-butyl)ammonium hexafluorophosphate ([<sup>n</sup>Bu<sub>4</sub>N]<sup>+</sup>[PF<sub>6</sub>]<sup>-</sup>; Sigma-Aldrich,  
441 electrochemical grade) served as the supporting electrolyte. Measurements were carried out with  
442 Gamry Reference 600+ Potentiostat/Galvanostat using a standard three-electrode configuration. The  
443 working electrode was the basal plane of highly oriented pyrolytic graphite (HOPG)  
444 (GraphiteStore.com, Buffalo Grove, Ill.; surface area: 0.09 cm<sup>2</sup>), the counter electrode was a platinum  
445 wire (Kurt J. Lesker, Jefferson Hills, PA; 99.99%, 0.5 mm diameter), and a silver wire immersed in  
446 electrolyte solution served as a pseudo-reference electrode (CH instruments). The reference was  
447 separated from the working solution by a Vycor frit (Bioanalytical Systems, Inc.). Ferrocene  
448 (Sigma-Aldrich; twice-sublimed) was added to the electrolyte solution at the end of each  
449 experiment; the midpoint potential of the ferrocenium/ferrocene couple (denoted as Fc<sup>+/-</sup>) was used  
450 as an external standard for comparison of the recorded potentials.

451 Concentrations of the analytes for cyclic voltammetry were typically 1 mM. Experiments were  
452 typically conducted by first scanning cathodically, then anodically on the return sweep.

453 Bulk electrolysis experiments were performed in a custom two-chamber electrochemical cell  
454 equipped with connections to achieve gas-tight operation. The working electrode was an HOPG

455 plate (Graphitestore.com, Buffalo Grove, Ill.; surface area: 10 cm<sup>2</sup>). 10 equiv. of ferrocene served as  
456 the sacrificial reductant.

457 *5.4. Spectroelectrochemistry*

458 Spectroelectrochemistry was carried out in the same glovebox as described above (N<sub>2</sub>  
459 atmosphere), with 0.10 M [<sup>t</sup>Bu<sub>4</sub>N][PF<sub>6</sub>] in THF as electrolyte. A thin layer quartz cell was used with  
460 a Teflon cap for housing the electrodes (ALS Co., Ltd., path length: 1.0 mm). The working electrode  
461 was a platinum mesh/flag electrode covered with a PTFE shrink tube up to the flag, and the counter  
462 electrode was a platinum wire (ALS Co., Ltd.).

463 *5.5. Gas Chromatography*

464 Gas chromatography were collected with a Shimadzu GC-2014 CustomGC. The instrument  
465 was calibrated with a standard checkout gas mixture (Agilent 5190-0519) prior to experimental runs  
466 to obtain quantitative data for H<sub>2</sub> and other gases. Calibration curves over a range of 100-10,000  
467 ppm were constructed with prepared mixture of H<sub>2</sub> and N<sub>2</sub> to enable H<sub>2</sub> quantification.

468 *5.6. Preparation of [Cp<sup>\*</sup>Rh(4,4'-dinitro-2,2'-bipyridyl)Cl]PF<sub>6</sub> (3)*

469 THF solutions of dnbpyp (0.0249 g, 0.101 mmol, 2 equiv.) and AgPF<sub>6</sub> (0.026 g, 0.103 mmol, 2  
470 equiv.) were added in sequence to a suspension of [Cp<sup>\*</sup>RhCl<sub>2</sub>]<sub>2</sub> (0.0314 g, 0.051 mmol, 1 equiv.) in  
471 THF. A gradual color change occurred over 20 minutes from dark red to bright yellow and a  
472 precipitate appeared. This suspension was filtered over Celite, and a homogeneous yellow solution  
473 was obtained. Trituration with approximately 50 mL Et<sub>2</sub>O resulted in formation of a bright yellow  
474 solid. The solution was decanted and excess solvent pumped off to obtain **3** (0.0294 g, 44% yield).  
475 Crystals suitable for X-ray diffraction analysis were obtained by vapor diffusion of Et<sub>2</sub>O into a  
476 solution of **3** in acetonitrile. <sup>1</sup>H NMR (500 MHz, CD<sub>3</sub>CN) δ 9.31 (d, <sup>4</sup>J<sub>H,H</sub> = 2.3 Hz, 2H), 9.23 (d, <sup>3</sup>J<sub>H,H</sub> =  
477 6.0, 2H), 8.52 (dd, <sup>4</sup>J<sub>H,H</sub> = 2.2, <sup>3</sup>J<sub>H,H</sub> = 6.0 Hz, 2H), 1.73 (s, 15H) ppm. <sup>13</sup>C{<sup>1</sup>H} NMR (126 MHz, CD<sub>3</sub>CN)  
478 δ 156.90, 156.49, 155.49, 123.01, 119.36, 99.69 (d, <sup>1</sup>J<sub>C,Rh</sub> = 8.26 Hz), 9.26 ppm. <sup>31</sup>P{<sup>1</sup>H} NMR (162 MHz,  
479 CD<sub>3</sub>CN) δ -146.88 (sept, <sup>1</sup>J<sub>P,F</sub> = 706.3 Hz). <sup>19</sup>F NMR (376 MHz, CD<sub>3</sub>CN) δ -72.9 (d, <sup>1</sup>J<sub>F,P</sub> = 707.0 Hz).  
480 Electronic absorption spectrum (THF): 239 (36400), 323 (13000), 365 nm (5300 M<sup>-1</sup> cm<sup>-1</sup>). ESI-MS  
481 (positive) *m/z*: 519.03 [3 - PF<sub>6</sub>]<sup>+</sup>.

482 Elemental analysis for a sample of **3** found 37.20% carbon, 4.43% hydrogen, and 7.78%  
483 nitrogen. Calculated values were 36.14%, 3.18%, and 8.43% respectively. Inclusion of trace THF  
484 associated with the isolated powder (0.3 eq.) provides the appropriate analysis values of 37.20%,  
485 3.46%, and 8.13% respectively. These are within 0.4% error of the analytical results and are  
486 consistent with isolation of solid **3** from THF.

487 *5.7. Generation and isolation of [Cp<sup>\*</sup>Rh(4,4'-dinitro-2,2'-bipyridyl)(L)]<sup>+</sup> (4)*

488 A solution of cobaltocene (0.0142, 0.075 mmol, 2 equiv.) in THF was added dropwise to a THF  
489 solution of **3** (0.0250 g, 0.037 mmol, 1 equiv.) while stirring. The color immediately changed from a  
490 light yellow to a dark green. After stirring for 10 minutes, the solution was pumped down to obtain  
491 a dark solid. This was washed with pentane and Et<sub>2</sub>O. The resulting solid was again dissolved in  
492 THF and filtered over Celite to obtain a dark green homogeneous solution. Removal of volatiles  
493 gave **4** as a dark green solid (0.0156 g, 62% yield). Electronic absorption spectrum (THF): 264  
494 (28500), 304 (6000), 418 (5200), 693 (13000), 860 (6000), 944 (7800 M<sup>-1</sup> cm<sup>-1</sup>).

495 **Supplementary Materials:** Supporting information is available online at [www.mdpi.com/xxx/s1](http://www.mdpi.com/xxx/s1), and includes:  
496 NMR spectra; crystallographic details; electronic absorption spectra; electrochemical, spectroelectrochemical,  
497 and gas chromatography data (PDF); cartesian coordinates (XYZ).

498 **Author Contributions:** Conceptualization, W.C.H., D.L. and J.D.B.; Data curation, V.W.D.; Investigation,  
499 W.N.G.M.; Supervision, W.C.H., D.L., and J.D.B.; Writing – original draft, J.D.B.; Writing – review & editing,  
500 W.N.G.M, D.L., and J.D.B..

501 **Funding:** This work was supported by the US National Science Foundation through award OIA-1833087.  
502 Support for preparation of 4,4'-dinitro-2,2'-bipyridyl was provided by the KU Hall Chemical Research Fund.  
503 W.N.G.M. acknowledges the Center for Undergraduate Research at the University of Kansas for support in the  
504 form of Undergraduate Research Awards. Support for the NMR instrumentation was provided by NIH Shared  
505 Instrumentation Grants (S10OD016360, S10RR024664) and NSF MRI funding (CHE-1625923). EPR spectra were  
506 collected at the Caltech EPR Facility.

507 **Acknowledgments:** The authors thank Keaton Prather for assistance with preparation of  
508 4,4'-dinitro-2,2'-bipyridyl, Dr. Paul Oyala and Prof. Emmanuelle Despagnet-Ayoub for assistance with EPR  
509 spectroscopy, and Dr. Justin Douglas and Sarah Neuenschwander for assistance with NMR spectroscopy.

510 **Conflicts of Interest:** The authors declare no conflict of interest.

511 **Sample Availability:** Samples of compounds **1**, **2**, and **3** are available from the authors upon request.



512 © 2018 by the authors. Submitted for possible open access publication under the terms  
513 and conditions of the Creative Commons Attribution (CC BY) license  
514 (<http://creativecommons.org/licenses/by/4.0/>).

515

## References

- <sup>1</sup> Meyer, T. J., Chemical approaches to artificial photosynthesis. *Acc. Chem. Res.* **1989**, *22*, 163-170.
- <sup>2</sup> Sattler, A.; VanderVelde, D. G.; Labinger, J. A.; Bercaw, J. E., Lewis Acid Promoted Titanium Alkylidene Formation: Off-Cycle Intermediates Relevant to Olefin Trimerization Catalysis. *J. Am. Chem. Soc.* **2014**, *136*, 10790-10800.
- <sup>3</sup> Vaska, L., Reversible activation of covalent molecules by transition-metal complexes. The role of the covalent molecule. *Acc. Chem. Res.* **1968**, *1*, 335-344.
- <sup>4</sup> Costentin, C.; Robert, M.; Saveant, J.-M., Catalysis of the electrochemical reduction of carbon dioxide. *Chem. Soc. Rev.* **2013**, *42*, 2423-2436.
- <sup>5</sup> (a) Lewis, N. S.; Nocera, D. G., Powering the planet: Chemical challenges in solar energy utilization. *Proc. Nat. Acad. Sci. U.S.A.* **2006**, *103*, 15729-15735. (b) Mayer, J. M., Understanding Hydrogen Atom Transfer: From Bond Strengths to Marcus Theory. *Acc. Chem. Res.* **2011**, *44*, 36-46.
- <sup>6</sup> Grills, D. C.; Polyansky, D. E.; Fujita, E., Application of Pulse Radiolysis to Mechanistic Investigations of Catalysis Relevant to Artificial Photosynthesis. *ChemSusChem* **2017**, *10*, 4359-4373.
- <sup>7</sup> Kölle, U.; Grätzel, M., Organometallic Rhodium(III) Complexes as Catalysts for the Photoreduction of Protons to Hydrogen on Colloidal TiO<sub>2</sub>. *Angew. Chem. Int. Ed. Engl.* **1987**, *26*, 567-570.
- <sup>8</sup> Kölle, U.; Kang, B. S.; Infelta, P.; Comte, P.; Grätzel, M., Electrochemical and pulse-radiolytic reduction of (pentamethylcyclopentadienyl)(polypyridyl)rhodium complexes. *Chem. Ber.* **1989**, *122*, 1869-80.
- <sup>9</sup> Henke, W. C.; Lionetti, D.; Moore, W. N. G.; Hopkins, J. A.; Day, V. W.; Blakemore, J. D., Ligand Substituents Govern the Efficiency and Mechanistic Path of Hydrogen Production with [Cp<sup>\*</sup>Rh] Catalysts. *ChemSusChem* **2017**, *10* (22), 4589-4598.
- <sup>10</sup> White, C.; Yates, A.; Maitlis, P. M., ( $\eta^5$ -Pentamethylcyclopentadienyl)Rhodium and -Iridium Compounds. *Inorg. Synth.* **1992**, *29*, 228-234.
- <sup>11</sup> Nutton, A.; Bailey, P. M.; Maitlis, P. M., Pentamethylcyclopentadienylrhodium and -iridium complexes. Part 29. Syntheses and x-ray structure determinations of tri-micro -hydroxybis[(h-pentamethylcyclopentadienyl)rhodium] hydroxide undecahydrate and -iridium acetate tetradecahydrate and related complexes. *J. Chem. Soc. Dalton Trans.* **1981**, 1997-2002.
- <sup>12</sup> Chardon-Noblat, S.; Cosnier, S.; Deronzier, A.; Vlachopoulos, N., An International Journal Devoted to all Aspects of Electrode Kinetics, Interfacial Structure, Properties of Electrolytes, Colloid and Biological ElectrochemistryElectrochemical properties of [(C<sub>5</sub>Me<sub>5</sub>)RhIII(L)Cl]<sup>+</sup> complexes (L = 2,2'-bipyridine or 1,10-phenanthroline derivatives) in solution in related polypyrrolic films. Application to electrocatalytic hydrogen generation. *J. Electroanal. Chem.* **1993**, *352*, 213-228.
- <sup>13</sup> Ruppert, R.; Herrmann, S.; Steckhan, E., Efficient indirect electrochemical in situ regeneration of NADH: electrochemically driven enzymatic reduction of pyruvate catalyzed by D-LDH. *Tet. Lett.* **1987**, *28*, 6583-6586.
- <sup>14</sup> Saveant, J.-M., *Elements of Molecular and Biomolecular Electrochemistry*. Wiley: Hoboken, NJ, 2006.

<sup>15</sup> Polyansky, D. E.; Muckerman, J. T.; Rochford, J.; Zong, R.; Thummel, R. P.; Fujita, E., Water Oxidation by a Mononuclear Ruthenium Catalyst: Characterization of the Intermediates. *J. Am. Chem. Soc.* **2011**, *133*, 14649-14665.

<sup>16</sup> Grills, D. C.; Polyansky, D. E.; Fujita, E., *ChemSusChem* **2017**, *10*, 4359-4373.

<sup>17</sup> Warren, J. J.; Tronic, T. A.; Mayer, J. M., Thermochemistry of Proton-Coupled Electron Transfer Reagents and its Implications. *Chem. Rev.* **2010**, *110*, 6961-7001.

<sup>18</sup> Appel, A. M.; Helm, M. L., Determining the Overpotential for a Molecular Electrocatalyst. *ACS Catalysis* **2013**, *4*, 630-633.

<sup>19</sup> Ladwig, M.; Kaim, W., Electronic structure of catalytic intermediates for production of hydrogen: (C<sub>5</sub>Me<sub>5</sub>)Ir(bpy) and its conjugated acid. *J. Organomet. Chem.* **1992**, *439*, 79-90.

<sup>20</sup> Kaim, W.; Reinhardt, R.; Waldhoer, E.; Fiedler, J., Electron transfer and chloride ligand dissociation in complexes [(C<sub>5</sub>Me<sub>5</sub>)ClM(bpy)]<sup>+</sup>/[(C<sub>5</sub>Me<sub>5</sub>)M(bpy)]<sup>n</sup> (M = Co, Rh, Ir; n = 2+, +, 0, -): A combined electrochemical and spectroscopic investigation. *J. Organomet. Chem.* **1996**, *524*, 195-202.

<sup>21</sup> Blakemore, J. D.; Hernandez, E. S.; Sattler, W.; Hunter, B. M.; Henling, L. M.; Brunschwig, B. S.; Gray, H. B., Pentamethylcyclopentadienyl rhodium complexes. *Polyhedron* **2014**, *84*, 14-18.

<sup>22</sup> Pitman, C. L.; Finster, O. N. L.; Miller, A. J. M., Cyclopentadiene-mediated hydride transfer from rhodium complexes. *Chem. Commun.* **2016**, *52*, 9105-9108.

<sup>23</sup> Quintana, L. M. A.; Johnson, S. I.; Corona, S. L.; Villatoro, W.; Goddard, W. A.; Takase, M. K.; VanderVelde, D. G.; Winkler, J. R.; Gray, H. B.; Blakemore, J. D., Proton-hydride tautomerism in hydrogen evolution catalysis. *Proc. Nat. Acad. Sci. U.S.A.* **2016**, *113*, 6409-6414.

<sup>24</sup> Peng, Y.; Ramos-Garcés, M. V.; Lionetti, D.; Blakemore, J. D., Structural and Electrochemical Consequences of [Cp<sup>\*</sup>] Ligand Protonation. *Inorg. Chem.* **2017**, *56*, 10824-10831.

<sup>25</sup> Boyd, E.A.; Lionetti, D.; Henke, W.C.; Day, V.W.; Blakemore, J.D., Preparation, Characterization, and Electrochemical Activation of a Model [Cp<sup>\*</sup>Rh] Hydride, *Inorg. Chem.* **2018**, Article ASAP, doi: 10.1021/acs.inorgchem.8b02160

<sup>26</sup> Hopkins, J.A., Lionetti, D., Day, V.W., and Blakemore, J.D., Chemical and Electrochemical Properties of [Cp<sup>\*</sup>Rh] Complexes Supported by a Hybrid Phosphine-Pyridine Ligand, **2018**, *in peer review*

<sup>27</sup> Chalkley, M. J.; Del Castillo, T. J.; Matson, B. D.; Roddy, J. P.; Peters, J. C., Catalytic N<sub>2</sub>-to-NH<sub>3</sub> Conversion by Fe at Lower Driving Force: A Proposed Role for Metallocene-Mediated PCET. *ACS Central Science* **2017**, *3*, 217-223.

<sup>28</sup> Pal, S.; Kusumoto, S.; Nozaki, K., Dehydrogenation of Dimethylamine-Borane Catalyzed by Half-Sandwich Ir and Rh Complexes: Mechanism and the Role of Cp<sup>\*</sup> Noninnocence. *Organometallics* **2018**, *37*, 906-914.

<sup>29</sup> Hansch, C.; Leo, A.; Taft, R. W., A survey of Hammett substituent constants and resonance and field parameters. *Chem. Rev.* **1991**, *91*, 165-195.

<sup>30</sup> Hildebrand, F.; Kohlmann, C.; Franz, A.; Luetz, S., Synthesis, characterization and application of new rhodium complexes for indirect electrochemical cofactor regeneration. *Adv. Synth. Catal.* **2008**, *350*, 909-918.

<sup>31</sup> Ziessel, R., Photocatalysis of water gas shift reactions under normal conditions with cationic iridium(III) complexes. *Angew. Chem.* **1991**, *103*, 863-866.

<sup>32</sup> Ziessel, R., Photocatalysis. Mechanistic studies of homogeneous photochemical water gas shift reaction catalyzed under mild conditions by novel cationic iridium(III) complexes. *J. Am. Chem. Soc.* **1993**, *115*, 118-27.

<sup>33</sup> Brereton, K. R.; Bellows, S. M.; Fallah, H.; Lopez, A. A.; Adams, R. M.; Miller, A. J. M.; Jones, W. D.; Cundari, T. R., Aqueous Hydricity from Calculations of Reduction Potential and Acidity in Water. *J. Phys. Chem. B* **2016**, *120*, 12911-12919.

<sup>34</sup> Ribeiro, P. E. A.; Donnici, C. L.; Dos Santos, E. N., Cationic rhodium(I) complexes containing 4,4'-disubstituted 2,2'-bipyridines: A systematic variation on electron density over the metal center. *J. Organomet. Chem.* **2006**, *691*, 2037-2043.

<sup>35</sup> Peng, Q.; Yan, H.; Zhang, X.; Wu, Y.-D., Conjugate Addition vs Heck Reaction: A Theoretical Study on Competitive Coupling Catalyzed by Isoelectronic Metal (Pd(II) and Rh(I)). *J. Org. Chem.* **2012**, *77*, 7487-7496.

<sup>36</sup> Pahls, D. R.; Groves, J. T.; Gunnoe, T. B.; Cundari, T. R., Theoretical Study of Reductive Functionalization of Methyl Ligands of Group 9 Complexes Supported by Two Bipyridyl Ligands: A Key Step in Catalytic Hydrocarbon Functionalization. *Organometallics* **2014**, *33*, 1936-1944.

<sup>37</sup> O'Reilly, M. E.; Pahls, D. R.; Cundari, T. R.; Gunnoe, T. B., Reductive Functionalization of a Rhodium(III)-Methyl Bond in Acidic Media: Key Step in the Electrophilic Functionalization of Methane. *Organometallics* **2014**, *33*, 6504-6510.

<sup>38</sup> Farrell, K.; Melle, P.; Gossage, R. A.; Muller-Bunz, H.; Albrecht, M., Transfer hydrogenation with abnormal dicarbene rhodium(III) complexes containing ancillary and modular poly-pyridine ligands. *Dalton Trans.* **2016**, *45*, 4570-4579.

<sup>39</sup> Muckerman, J. T.; Skone, J. H.; Ning, M.; Wasada-Tsutsui, Y., Toward the accurate calculation of pKa values in water and acetonitrile. *Biochim. Biophys. Acta Bioenerg.* **2013**, *1827*, 882-891.

<sup>40</sup> Lionetti, D.; Day, V. W.; Lassalle-Kaiser, B.; Blakemore, J. D., Multiple binding modes of an unconjugated bis(pyridine) ligand stabilize low-valent [Cp<sup>\*</sup>Rh] complexes. *Chem. Comm.* **2018**, *54*, 1694-1697.

<sup>41</sup> Lionetti, D.; Day, V. W.; Blakemore, J. D., Synthesis and Electrochemical Properties of Half-Sandwich Rhodium and Iridium Methyl Complexes. *Organometallics* **2017**, *36*, 1897-1905.

<sup>42</sup> Simpson, P. G.; Vinciguerra, A.; Quagliano, J. V., The donor properties of 2,2'-bipyridine N,N'-dioxide. *Inorg. Chem.* **1963**, *2*, 282-286.

<sup>43</sup> (a) Maerker, G.; Case, F. H., The Synthesis of Some 4,4'-Disubstituted 2,2'-Bipyridines1. *J. Am. Chem. Soc.* **1958**, *80*, 2745-2748. (b) Kavanagh, P.; Leech, D., Improved synthesis of 4,4'-diamino-2,2'-bipyridine from 4,4'-dinitro-2,2'-bipyridine-N,N'-dioxide. *Tet. Lett.* **2004**, *45*, 121-123. (c) Zhang, D.; Telo, J. P.; Liao, C.; Hightower, S. E.; Clennan, E. L., Experimental and Computational Studies of Nuclear Substituted 1,1'-Dimethyl-2,2'-Bipyridinium Tetrafluoroborates. *J. Phys. Chem. A* **2007**, *111*, 13567-13574.

<sup>44</sup> (a) Wenkert, D.; Woodward, R. B., Studies of 2,2'-bipyridyl N,N'-dioxides. *J. Org. Chem.* **1983**, *48*, 283-289. (b) ten Brink, G.-J.; Arends, I.W.C.E.; Hoogenraad, M.; Verspui, G.; Sheldon, R.A., Catalytic Conversions in Water. Part 22: Electronic Effects in the (Diimine)palladium(II)-Catalysed Aerobic Oxidation of Alcohols. *Adv. Synth. Catal.* **2003**, *345*, 497-505.

<sup>45</sup> Groom, C. R.; Bruno, I. J.; Lightfoot, M. P.; Ward, S. C., The Cambridge Structural Database. *Acta Cryst. Sec. B* **2016**, *72*, 171-179.

<sup>46</sup> Pilkington, M.; Capelli, S.; Hauser, J.; Hoffmann, C.; Burgi, H.-B., 4,4'-Dinitro-2,2'-bipyridine. *Acta Cryst. Sec. C* **1997**, *53*, 1719-1721.

<sup>47</sup> (a) Kinnunen, T.-J. J.; Haukka, M.; Nousiainen, M.; Patrikka, A.; Pakkanen, T. A., Electron withdrawing and electron donating effects of 4,4'[prime or minute]-bipyridine substituents on ruthenium mono(bipyridine) complexes. *J. Chem. Soc. Dalton Trans.* **2001**, 2649-2654. (b) Moore, M.; Knight, D. A.; Zabetakis, D.; Deschamps, J. R.; Dressick, W. J.; Chang, E. L.; Lascano, B.; Nita, R.; Trammell, S. A., Electronic effects on the reactivity of copper mono-bipyridine complexes. *Inorg. Chem. Acta* **2012**, *388*, 168-174. (c) McKeown, B. A.; Gonzalez, H. E.; Friedfeld, M. R.; Brosnahan, A. M.; Gunnoe, T. B.; Cundari, T. R.; Sabat, M., Platinum(II)-Catalyzed Ethylene Hydrophenylation: Switching Selectivity between Alkyl- and Vinylbenzene Production. *Organometallics* **2013**, *32* (9), 2857-2865. (d) S. Parsons, L. Yellowlees, P.A. Wood CCDC 247862: Experimental Crystal Structure Determination, **2014**, DOI: 10.5517/cc89xk0. (e) A.Yu. Kovalevsky, P. Coppens CCDC 179657: Experimental Crystal Structure Determination, **2014**, DOI: 10.5517/cc60ydj. (f) Weber, M. D.; Viciana-Chumillas, M.; Armentano, D.; Cano, J.; Costa, R. D., [sigma]-Hammett parameter: a strategy to enhance both photo- and electro-luminescence features of heteroleptic copper(I) complexes. *Dalton Trans.* **2017**, *46*, 6312-6323.

<sup>48</sup> There is a slight shift of the measured reduction potentials to more positive values (ca. 150-200 mV versus  $\text{Fc}^{+/-}$ ) for all four redox events (see SI, Figure S10). Such solvent-dependent potential shifts are difficult to interpret reliably, although this shift may be explained by solvation effects that affect the  $\text{Fc}^{+/-}$  couple in these two solvents (+0.40 V vs. SCE in MeCN vs. +0.56 V vs. SCE in THF). See reference 49 for further discussion.

<sup>49</sup> Connelly, N. G.; Geiger, W. E., Chemical Redox Agents for Organometallic Chemistry. *Chem. Rev.* **1996**, *96*, 877-910.

<sup>50</sup> De Bruin, B.; Hetterscheid, D. G. H.; Koekkoek, A. J. J.; Grützmacher, H. In *Progress in Inorganic Chemistry*; John Wiley & Sons, Inc.: 2008; Vol. 55, p 247-354.

<sup>51</sup> (a) Creutz, C., Bipyridine radical ions. *Comments Inorg. Chem.* **1982**, *1*, 293-311. (b) Shida, T. *Electronic Absorption Spectra of Radical Ions*; Elsevier: Amsterdam ; New York, 1988.

<sup>52</sup> Coombe, V. T.; Heath, G. A.; MacKenzie, A. J.; Yellowlees, L. J., Spectroelectrochemical studies on tris(bipyridyl)iridium complexes: ultraviolet, visible and near-infrared spectra of the series  $[\text{Ir}(\text{bipyridyl})_3]^{3+/2+/+/-}$ . *Inorg. Chem.* **1984**, *23*, 3423-3425.

<sup>53</sup> Murray, P. R.; Crawford, S.; Dawson, A.; Delf, A.; Findlay, C.; Jack, L.; McInnes, E. J. L.; Al-Musharafi, S.; Nichol, G. S.; Oswald, I.; Yellowlees, L. J., On the electronic structure of nitro-substituted bipyridines and their platinum complexes. *Dalton Trans.* **2012**, *41*, 201-207.

---

<sup>54</sup> Fulmer, G. R.; Miller, A. J. M.; Sherden, N. H.; Gottlieb, H. E.; Nudelman, A.; Stoltz, B. M.; Bercaw, J. E.; Goldberg, K. I., NMR Chemical Shifts of Trace Impurities: Common Laboratory Solvents, Organics, and Gases in Deuterated Solvents Relevant to the Organometallic Chemist. *Organometallics* **2010**, *29*, 2176-2179.

<sup>55</sup> (a) Harris, R. K.; Becker, E. D.; Cabral De Menezes, S. M.; Goodfellow, R.; Granger, P., NMR nomenclature. Nuclear spin properties and conventions for chemical shifts (IUPAC recommendations 2001). *Pure Appl. Chem.* **2001**, *73*, 1795-1818. (b) Harris, R. K.; Becker, E. D.; Cabral De Menezes, S. M.; Granger, P.; Hoffman, R. E.; Zilm, K. W., Further conventions for NMR shielding and chemical shifts: (IUPAC recommendations 2008). *Pure Appl. Chem.* **2008**, *80*, 59-84.